Constrained Pole Placement Optimization Using the Flower Pollination Algorithm for Velocity Tracking of Differential-Drive Mobile Robots

Anh-Minh Duc Tran
Modeling Evolutionary Algorithms Simulation and Artificial Intelligence, Faculty of Electrical and Electronics Engineering, Ton Duc Thang University, Ho Chi Minh City, Vietnam
tranducanhminh@tdtu.edu.vn (corresponding author)

Tri-Vien Vu
Modeling Evolutionary Algorithms Simulation and Artificial Intelligence, Faculty of Electrical and Electronics Engineering, Ton Duc Thang University, Ho Chi Minh City, Vietnam
vutrivien@tdtu.edu.vn

Received: 15 March 2026 | Revised: 11 May 2026, 29 May 2026, and 8 June 2026 | Accepted: 9 June 2026

 DOI: https://doi.org/10.48084/etasr.18761

ABSTRACT

This paper proposes a Flower Pollination Algorithm (FPA)-based constrained pole-placement framework for velocity-tracking control of Differential-Drive Mobile Robots (DDMRs) subject to actuator-voltage limitations and external disturbances. A fourth-order state-space model is derived from Newton-Euler principles, including coupled electromechanical dynamics and disturbance inputs. The pole-placement problem is formulated as a constrained multi-objective optimization task balancing tracking performance, Cross-Coupling (CC) reduction, and actuator saturation penalties. A reference prefilter is included to improve nominal steady-state tracking, while closed-loop stability is ensured by restricting the poles to the open left-half plane. The proposed controller is compared with classical pole placement, Linear Quadratic Regulator (LQR), and Model Reference Adaptive Control (MRAC). The simulation results show that although LQR achieves good nominal tracking, it requires 102.9 V, exceeding the 48 V actuator limit, whereas MRAC exhibits higher tracking errors and severe cross-coupling (CC = 1.94). In contrast, the proposed method maintains a feasible control effort while achieving satisfactory tracking performance under external disturbances.

Keywords-constrained pole placement; differential-drive mobile robots; flower pollination algorithm; actuator saturation; velocity tracking; cross-coupling analysis

I. INTRODUCTION

Differential-Drive Mobile Robots (DDMRs) are widely used in autonomous transportation and warehouse logistics because of their simple structure and high maneuverability [1, 2]. Coordinated DDMR fleets can improve material-handling efficiency in warehouse environments [3]. However, precise velocity tracking is challenging due to modeling uncertainties and physical constraints.

Various control strategies have been investigated for DDMR tracking and regulation, including neural-network-based [4], nonlinear [5], and sliding-mode controllers [6]. Classical pole placement ensures nominal stability but lacks a systematic mechanism for handling constraints in multivariable systems [7]. Linear Quadratic Regulator (LQR) provides structured weighting but may be sensitive to model mismatch. Fuzzy and adaptive controllers have also been investigated to improve tracking robustness under uncertainties [8, 9].

However, many existing pole-placement and optimal control designs neglect the 48 V saturation limit of industrial motor drivers and the coupling between translational and rotational dynamics [10, 11]. Ignoring such constraints may lead to physically unrealizable control actions. Although saturation-aware [12] and anti-windup designs [13] have been investigated, they often require additional tuning complexity.

To address these limitations, the current study proposes an FPA-based constrained pole-placement framework in which pole selection is formulated as a multi-objective optimization problem balancing tracking performance, Cross-Coupling (CC) reduction, and actuator saturation penalties under the 48 V limit [14, 15]. Metaheuristic optimizers, such as GA, PSO, and DE,

have also been widely investigated for controller-parameter tuning and related engineering optimization tasks [14].

The main contributions of the current study are:

- a multi-objective formulation balancing tracking and actuator saturation
- an FPA-based constrained pole-selection framework
- a comparative evaluation using Root Mean Square Error (RMSE), voltage feasibility, and DC-gain CC metrics.

II. SYSTEM MODELING

A. DDMR Dynamics

This subsection derives the differential equations of the DDMR from the input voltages V_{aR} and V_{aL} to the longitudinal velocity V and yaw rate ω_z. The derivation follows the modeling framework in [16]. The DDMR schematic, including coordinate systems and disturbances, is shown in Figure 1. The model assumes that the center of gravity is located at the geometric midpoint, pure rolling occurs without slipping [1], and the left and right motors may have different parameters.

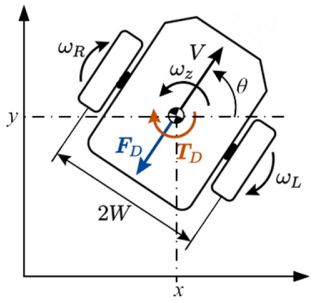

Fig. 1. Schematic representation of the DDMR showing wheel angular velocities, body velocity, yaw motion, and external disturbances.

1) Robot Body Dynamics (Newton-Euler)

Applying Newton's second law for translation and rotation about the Center of Gravity leads to dynamic equations based on rigid-body mechanics:

$$F_R + F_L = m\dot{V} \tag{1}$$

$$(F_R - F_L)W = J_z\dot{\omega}_z \Rightarrow F_R - F_L = \frac{J_z}{W}\dot{\omega}_z \tag{2}$$

2) Kinematic Relations

Under the no-slip condition and gearbox reduction [1, 16]:

$$V = \frac{R_{wR}\omega_R}{2i_{gR}} + \frac{R_{wL}\omega_L}{2i_{gL}}, \omega_z = \frac{R_{wR}\omega_R}{2Wi_{gR}} - \frac{R_{wL}\omega_L}{2Wi_{gL}} \tag{3}$$

Differentiating with respect to time:

$$\dot{V} = \frac{R_{wR}\dot{\omega}_R}{2i_{gR}} + \frac{R_{wL}\dot{\omega}_L}{2i_{gL}}, \dot{\omega}_z = \frac{R_{wR}\dot{\omega}_R}{2Wi_{gR}} - \frac{R_{wL}\dot{\omega}_L}{2Wi_{gL}} \tag{4}$$

3) Motor Dynamics

The DC motor dynamics are:

$$L_{aR}\dot{i}_{aR} = -R_{aR}i_{aR} - K_{tR}\omega_R + V_{aR} \tag{5}$$

$$L_{aL}\dot{i}_{aL} = -R_{aL}i_{aL} - K_{tL}\omega_L + V_{aL} \tag{6}$$

$$J_R\dot{\omega}_R = K_{tR}i_{aR} - \frac{F_R R_{wR}}{i_{gR}\eta_{gR}} - B_{mR}\omega_R \tag{7}$$

$$J_L\dot{\omega}_L = K_{tL}i_{aL} - \frac{F_L R_{wL}}{i_{gL}\eta_{gL}} - B_{mL}\omega_L \tag{8}$$

4) Traction Forces and Coupled Inertia

Substituting (4) into (1, 2) and then into (7, 8) yields the dynamics in terms of the inertia matrix **M**:

$$\mathbf{M}\begin{bmatrix}\dot{\omega}_R \\ \dot{\omega}_L\end{bmatrix} = \begin{bmatrix}K_{tR}i_{aR} & -B_{mR}\omega_R \\ K_{tL}i_{aL} & -B_{mL}\omega_L\end{bmatrix}, \mathbf{M} = \begin{bmatrix}C_R & C_{RL} \\ C_{LR} & C_L\end{bmatrix} \tag{9}$$

where the inertia and coupling coefficients are:

$$C_R = J_R + \frac{R_{wR}^2}{i_{gR}^2}\left(\frac{m}{4} + \frac{J_z}{4W^2}\right) \tag{10}$$

$$C_{RL} = \frac{R_{wR}R_{wL}}{i_{gR}i_{gL}}\left(\frac{m}{4} - \frac{J_z}{4W^2}\right) \tag{11}$$

$$C_L = J_L + \frac{R_{wL}^2}{i_{gL}^2}\left(\frac{m}{4} + \frac{J_z}{4W^2}\right) \tag{12}$$

$$C_{LR} = C_{RL} \tag{13}$$

The equivalent inertia terms include an effective wheel inertia coefficient that represents the inertia distribution of the lightweight wheel structure and drivetrain in the electromechanical model.

Inverting **M** with determinant $\Delta = C_R C_L - C_{RL}^2$ gives:

$$\dot{i}_{aR} = k_{1R}i_{aR} + k_{2R}\omega_R + k_{3R}V_{aR} \tag{14}$$

$$\dot{\omega}_R = k_{4R}i_{aR} - k_{5R}\omega_R - k_{6R}i_{aL} + k_{7R}\omega_L \tag{15}$$

$$\dot{i}_{aL} = k_{1L}i_{aL} + k_{2L}\omega_L + k_{3L}V_{aL} \tag{16}$$

$$\dot{\omega}_L = -k_{6L}i_{aR} + k_{7L}\omega_R + k_{4L}i_{aL} - k_{5L}\omega_L \tag{17}$$

where the coefficients k_i are:

$$k_{1R} = -R_{aR}/L_{aR}, k_{2R} = -K_{tR}/L_{aR}, k_{3R} = 1/L_{aR},$$

$$k_{4R} = C_L K_{tR}/\Delta, k_{5R} = C_L B_{mR}/\Delta,$$

$$k_{6R} = C_{RL}K_{tL}/\Delta, k_{7R} = C_{RL}B_{mL}/\Delta.$$

B. State-Space Representation

Equations (14-17) are written in state-space form with $\mathbf{x} = [i_{aR}, \omega_R, i_{aL}, \omega_L]^T$, $\mathbf{u} = [V_{aR}, V_{aL}]^T$, and $\mathbf{y} = [V, \omega_z]^T$:

$$\dot{\mathbf{x}} = \mathbf{Ax} + \mathbf{Bu}, \mathbf{y} = \mathbf{Cx} \tag{18}$$

For the nominal symmetric DDMR, the matrices **A**, **B**, **C** are derived from the parameters outlined in Table I. The system is controllable and observable for the nominal parameter set. Since (**A** - **BK**) is Hurwitz, the closed-loop system is asymptotically stable [17]. Under bounded disturbances **d,** the closed-loop states remain bounded according to the standard bounded-input bounded-state stability theory.

For robustness analysis, external force and torque disturbances are applied to the robot body: $F_R + F_L + F_D = m\dot{V}$ and $(F_R - F_L)W + T_D = J_z\dot{\omega}_z$. The resulting augmented state-space model is:

$$\dot{\mathbf{x}} = \mathbf{Ax} + \mathbf{Bu} + \mathbf{B}_d\mathbf{d} \tag{19}$$

where $\mathbf{d} = [F_D, T_D]^T$, and $\mathbf{B}_d$ is:

$$\mathbf{B}_d = \begin{bmatrix} 0 & 0 \\ \Gamma_{11} & \Gamma_{12} \\ 0 & 0 \\ \Gamma_{21} & \Gamma_{22} \end{bmatrix} \quad (20)$$

where Γ_{ij} are the elements of $\mathbf{\Gamma} = \mathbf{M}^{-1}\mathbf{G}_d$, and $\mathbf{G}_d = \frac{R_w}{2 i_g \eta_g}\begin{bmatrix} 1 & -1/W \\ 1 & 1/W \end{bmatrix}$.

TABLE I. PHYSICAL PARAMETERS OF THE DDMR PLATFORM

Parameter	Value
Total mass m	21.0 kg
Moment of inertia J_z	0.35 kg·m^2
Base width $2W$	0.4 m
Wheel radius R_w	0.075 m
Gear ratio i_g	2.0
Gear efficiency η_g	0.85
Torque constant K_t	0.573 Nm/A
Viscous friction coefficient B_m	0.011 N·m·s
Armature resistance R_a	0.928 Ω
Armature inductance L_a	0.015 H
Equivalent shaft inertia J_{sh}	1.8×10^{-3} kg·m^2
Actuator-voltage limit u_{max}	48.0 V

III. CONTROL PROBLEM FORMULATION

For the controllable system in (18), pole placement assigns the closed-loop poles of $(\mathbf{A} - \mathbf{BK})$ through the state-feedback law $\mathbf{u} = -\mathbf{Kx}$ [7].

A. Limitations under Saturation

Although pole placement ensures nominal stability, several practical limitations remain, including multi-input state-feedback structures that restrict feasible pole assignments, classical designs that neglect the 48 V actuator limit, and inadequate consideration of the CC between velocity channels [7, 10].

B. Constrained Optimization Problem

To address these limitations, the pole-placement task is formulated as a constrained multi-objective optimization problem. A reference prefilter is included in the control law [18]:

$$\mathbf{u} = -\mathbf{Kx} + \mathbf{N}_r\mathbf{r} \quad (21)$$

where $\mathbf{N}_r$ ensures unity steady-state gain under nominal conditions. Candidate pole sets are evaluated using:

$$J(\boldsymbol{p}) = w_r \cdot J_{\mathrm{RMSE}} + w_{cc} \cdot J_{\mathrm{CC}} + w_u \cdot \mathrm{Sat\_Penalty} \quad (22)$$

where J_{RMSE} represents the tracking error, J_{CC} the CC index, and the saturation term penalizes the violations of the 48 V actuator limit:

$$\mathrm{Sat\_Penalty} = \sum_t \max(0, |u_i(t)| - 48)^2 \quad (23)$$

The resulting optimization problem is highly nonlinear due to the dependence of the closed-loop response on the pole locations and saturation constraints.

IV. PROPOSED FPA-BASED CONTROL DESIGN

A. Flower Pollination Algorithm

The Flower Pollination Algorithm (FPA) combines global Lévy-flight exploration with local neighborhood exploitation for controller optimization [15, 19]. The algorithm models global and local pollination processes inspired by natural flower pollination mechanisms.

FPA has been applied to multi-objective optimization problems with relatively few tunable parameters, mainly the switch probability p [15]. Applications in drive systems [20] and engineering optimization problems such as voltage stability optimization [21] motivate its use for the present constrained pole-search problem. Candidate solutions are updated through global and local pollination mechanisms [19]:

Global Pollination: $x_i^{t+1} = x_i^t + L(s,\lambda)(g^* - x_i^t)$, where $L(s,\lambda)$ denotes the Lévy-flight step size.

Local Pollination: $x_i^{t+1} = x_i^t + \epsilon\left(x_j^t - x_k^t\right)$, representing local solution perturbations.

The Lévy-flight step size is generated using the Mantegna algorithm, as described in [15]. The resulting constrained pole-selection procedure with closed-loop simulation and voltage-penalty evaluation is summarized in the following Algorithm:

Algorithm 1. Constrained FPA pole-selection procedure

- Input: **A**, **B**, **C**, pole bounds [−150, −5], population size N, maximum iterations N_{iter}, actuator-voltage limit u_{max} = 48 V.
- Output: **p***, **K***,$\mathbf{N}_r^*$.
- 1. Initialize N flower candidates as pole vectors within [-150, -5].
- 2. For each candidate **p**, compute **K** and $\mathbf{N}_r$, simulate the saturated closed-loop response, and evaluate J(**p**) using (22)-(23).
- 3. For k = 1, ..., N_{iter}, update candidates by global Lévy-flight or local pollination, project poles into [-150, -5], and re-evaluate J(**p**).
- 4. Penalize any voltage violation beyond u_{max} and update the global best solution.
- 5. Return **p***, **K***, and $\mathbf{N}_r^*$.

B. Constrained Pole Optimization

To enforce the 48 V actuator limit, the objective function in (22) uses $w_u = 10^6$ to strongly penalize the saturation violations defined in (23). The pole search is restricted to the real interval [-150, -5]. Since complex poles may produce underdamped oscillatory responses [7], only real poles are considered to promote smoother actuator responses in logistics platforms.

To account for physical hardware limits, the actual voltage applied to the motors is directly bounded by the saturation function, $\mathbf{u}_{applied} = \mathrm{sat}(\mathbf{u}, \pm 48)$, preventing excessive voltage commands.

C. Reference Prefilter Design

To improve nominal velocity tracking, a reference prefilter is incorporated into the state-feedback law. Standard state-feedback controllers may exhibit steady-state tracking errors for step inputs without integral action or prefilter compensation [18]. Following standard design principles [7], the prefilter:

$$\mathbf{N}_{\mathrm{r}} = -(\mathbf{C}(\mathbf{A}-\mathbf{BK})^{-1}\mathbf{B})^{-1} \quad (24)$$

which provides a unity steady-state gain from the reference command to the nominal output velocities, as illustrated in the control architecture in Figure 2.

The nominal closed-loop system is asymptotically stable if all poles satisfy $\mathrm{Re}(p_i) < 0$, such that $(\mathbf{A}-\mathbf{BK})$ is Hurwitz [7]. Since the prefilter is implemented as a static gain, it does not modify the closed-loop eigenvalues.

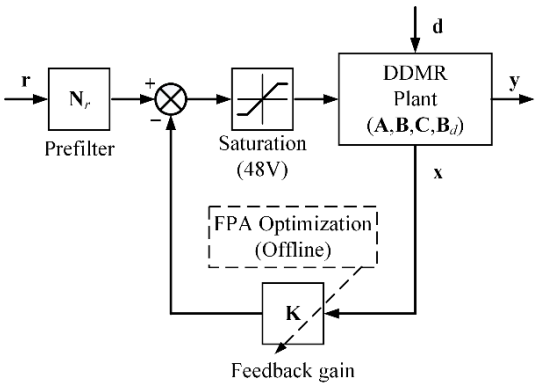

Fig. 2. Block diagram of the proposed constrained pole-placement control framework with reference prefilter and actuator saturation.

D. Cross-Coupling Reduction Metric

Differential-drive robots exhibit coupling between translational and rotational dynamics [16]. Previous studies using the Relative Gain Array (RGA) identified this interaction as a challenge for independent channel control [11]. A CC index based on the steady-state DC gain matrix is therefore adopted as an optimization objective:

$$\mathrm{CC} = \left\| \boldsymbol{G}_{cl} - \mathrm{diag}\big(\mathrm{diag}(\boldsymbol{G}_{cl})\big) \right\|_2 \quad (25)$$

Here, $\boldsymbol{G}_{cl}$ denotes the un-prefiltered closed-loop DC gain matrix; so, minimizing the CC index reduces the decoupling burden on the static prefilter $\mathbf{N}_{\mathrm{r}}$. Minimizing this DC-gain-based index reduces steady-state coupling between the linear and angular dynamics. However, transient coupling may still occur during abrupt maneuvers. The optimization is performed over 120 iterations using 40 flowers based on the objective function in (22).

V. SIMULATION ENVIRONMENT

A. Robot Parameters

The simulations used the nominal symmetric DDMR parameters in Table I, corresponding to a 21 kg logistics platform [16].

B. Simulation Setup

Simulations were performed in MATLAB R2025b using a fixed-step ODE4 solver with a 1 ms step size over 4 s. Multi-step velocity and yaw-rate reference signals were used to emulate logistics maneuvers. The simulation and FPA parameters are summarized in Table II.

TABLE II. SIMULATION SETTINGS AND FPA OPTIMIZATION PARAMETERS

Parameter	Value
Simulation step size dt	1 ms
Simulation duration T	4 s
Population size n	40
Maximum iterations N_{iter}	120
Switch probability p	0.8
Pole search interval	[-150, -5]
Weights $[w_r, w_{cc}]$	[1.0, 0.8]
Saturation penalty weight w_u	10^6

C. Benchmark Controllers

Three benchmark controllers were considered: classical PP with poles $\mathbf{p} = [-10, -20, -30, -40]$ [7]; LQR with $\mathbf{Q} = \mathrm{diag}(1,1,1,1)$ and $\mathbf{R} = 0.1 \times \mathbf{I}_2$, tuned without actuator constraints; and MRAC using normalized Lyapunov-based adaptation with $\gamma = \gamma_r = 0.5$ and reference model poles [-15.0, -15.1, -15.2, -15.3]. These benchmarks are included for qualitative comparative evaluation rather than exhaustive controller optimization.

D. Evaluation Metrics

Performance was evaluated using:

- RMSE for V and ω_z
- peak control voltage $u_{peak} = max|u_i|$ over the simulation
- The CC index
- Constraint satisfaction ($u_{peak} \leq u_{max} = 48\ V$).

Robustness tests included $\pm 10\%$ parameter variations, Gaussian noise ($\sigma = 0.01$), a 15 N longitudinal disturbance, and a 2.5 Nm torque pulse applied during t in [1.5, 2.5] s.

VI. RESULTS AND DISCUSSION

A. Optimization Results

The FPA converged to $\mathbf{p}^*$ = [-95.4,-94.4,-28.3,-145.9] within 80 iterations. Motivated by the use of alternative metaheuristics in controller tuning [14], Table III summarizes a limited five-run comparison of GA, PSO, and FPA under identical settings. Fitness values are reported as the mean ± standard deviation, whereas the RMSE, peak voltage, and CC index correspond to the best solution obtained by each optimizer.

Figure 3 shows that the best fitness stabilizes after approximately 20 iterations, while the mean fitness gradually decreases, indicating consistent convergence behavior.

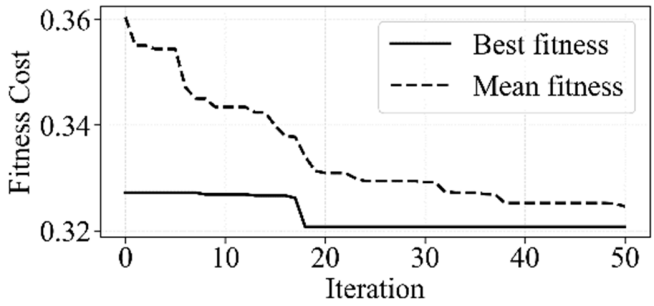

Fig. 3. Convergence history of the proposed FPA, showing the best and mean fitness values across optimization iterations.

All three optimizers found feasible pole configurations satisfying the 48 V constraint. PSO achieved the lowest mean fitness, whereas FPA obtained the lowest CC index and slightly lower peak voltage, indicating a competitive cross-coupling/actuator-feasibility trade-off, as illustrated in Table III.

TABLE III. LIMITED COMPARATIVE OPTIMIZATION RESULTS OVER FIVE INDEPENDENT RUNS

Opti-mizer	Fitness cost (mean ± std)	Best RMSE_V (m/s)	Best RMSE ω_z (rad/s)	Best peak voltage (V)	Best CC index
GA	0.3185 ± 0.0017	0.1429	0.1491	48.0	0.0308
PSO	0.3165 ± 0.0003	0.1481	0.1456	48.0	0.0281
FPA	0.3246 ± 0.0033	0.1539	0.1448	47.4	0.0275

B. Tracking Performance

The FPA-based controller achieved a low steady-state error in the multi-step reference scenario, as depicted in Figure 4, with a CC index of 0.0326. The corresponding disturbed-case tracking and control-voltage responses are presented in Figure 5.

C. Comparative, Robustness, and Control Effort Analysis

The voltage subplots of Figures 4 and 5 show that LQR exceeds the 48 V actuator limit during aggressive transients, whereas FPA remains within the admissible voltage range under nominal and disturbed conditions. As summarized in Table IV, LQR gives the lowest nominal RMSE but exceeds 100 V, whereas FPA maintains 46.6 V within the 48 V limit and improves tracking compared with classical PP. Under 15 N disturbances and sensor noise, FPA maintained RMSE below 0.17.

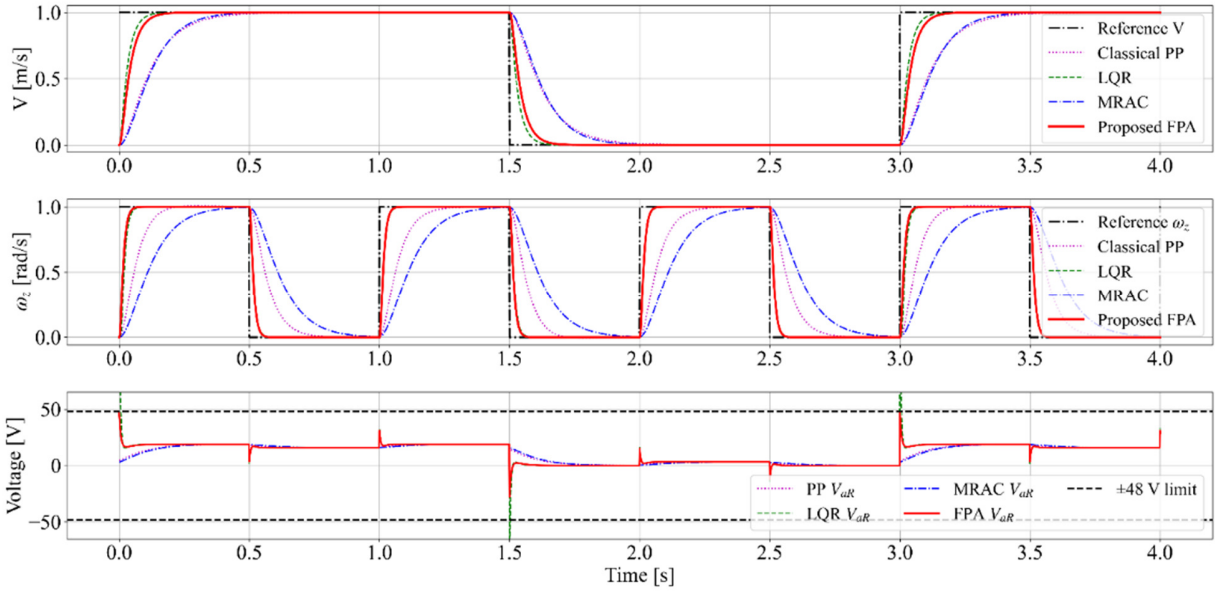

Fig. 4. Nominal velocity-tracking and control-voltage responses with the actuator-voltage limit indicated.

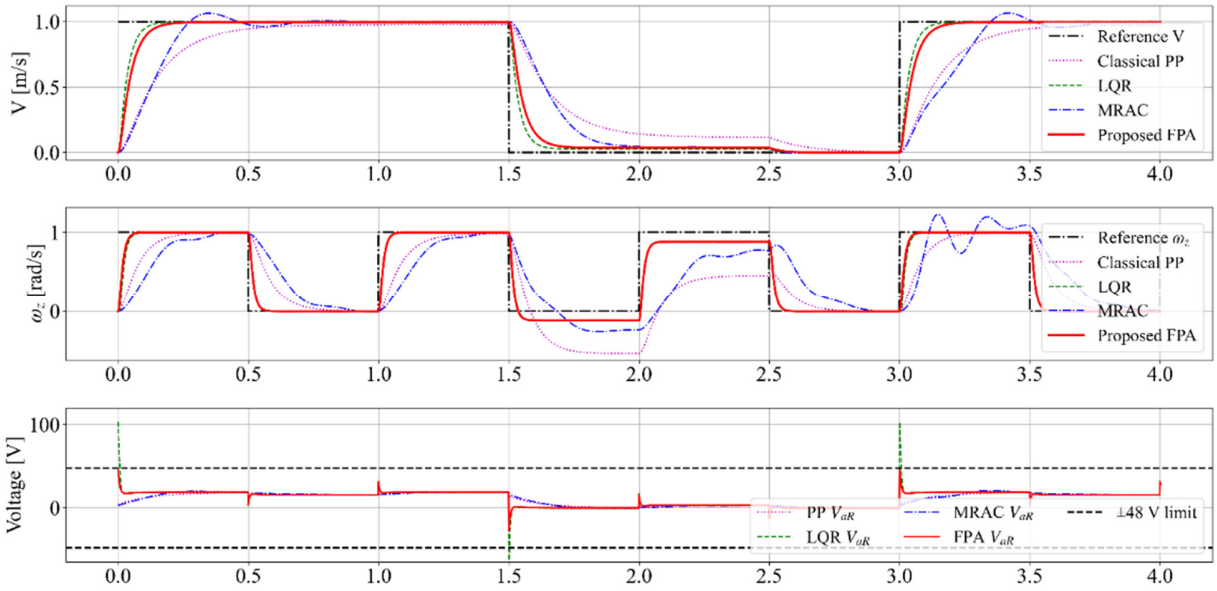

Fig. 5. Disturbed tracking and control-voltage responses for t ∈ [1.5, 2.5] s with the actuator-voltage limit indicated.

TABLE IV. COMPARATIVE PERFORMANCE UNDER NOMINAL AND DISTURBANCE CONDITIONS

Controller	RMSE V (m/s)	RMSE ω_z (rad/s)	Peak voltage (V)	CC Index	RMSE V (dist.) (m/s)	RMSE ω_z (dist.) (rad/s)
Classical PP	0.2437	0.3007	18.9	0.5477	0.2783	0.4111
LQR	0.1224	0.1595	102.9	0.0291	0.1295	0.1743
MRAC	0.2496	0.4055	18.9	1.9437	0.2767	0.4277
FPA (proposed)	0.1431	0.1512	46.6	0.0326	0.1533	0.1667

VII. CONCLUSION

This paper presented a Flower Pollination Algorithm (FPA)-based constrained pole-placement framework for Differential-Drive Mobile Robot (DDMR) velocity tracking under actuator-voltage limitations. The proposed design combines state-feedback pole placement, reference prefiltering, saturation penalties, and a DC-gain-based Cross-Coupling (CC) metric to address the gap between the nominal pole-placement design and the physically feasible actuator operation.

The simulation results show that the proposed controller provides a practical trade-off between tracking accuracy and actuator feasibility. Although Linear Quadratic Regulator (LQR) achieves the lowest nominal Root Mean Square Error (RMSE), it requires 102.9 V and violates the 48 V limit, whereas the proposed method maintains 46.6 V under nominal conditions and acceptable tracking performance under disturbances. The PSO/GA/FPA comparison further indicates that FPA remains competitive in the considered constrained pole-search setting.

This study remains simulation-based and limited to real-pole placement and selected benchmarks. Future work will address experimental or hardware-in-the-loop validation, longer-duration tracking, uncertainty tests, and extensions to complex-pole, damping-ratio-based, nonlinear, or adaptive constrained control formulations.

DECLARATION OF COMPETING INTERESTS

The authors declare no competing interests.

ACKNOWLEDGMENT

Not applicable to this work.

DATA AVAILABILITY

All data supporting this study are included in the article.

VIII. REFERENCES

[1] R. Siegwart, *Introduction to autonomous mobile robots*, 2nd ed. Cambridge, Massachusetts: MIT Press, 2011.

[2] A. D. Luca and G. Oriolo, "Modelling and Control of Nonholonomic Mechanical Systems," in *Kinematics and Dynamics of Multi-Body Systems*, vol. 360, J. Angeles and A. Kecskeméthy, Eds. Vienna: Springer Vienna, 1995, pp. 277-342, https://doi.org/10.1007/978-3-7091-4362-9_7.

[3] L. Wang and G. Liu, "Research on multi-robot collaborative operation in logistics and warehousing using A3C optimized YOLOv5-PPO model," *Frontiers in Neurorobotics*, vol. 17, Jan. 2024, Art. no. 1329589, https://doi.org/10.3389/fnbot.2023.1329589.

[4] N. Hassan and A. Saleem, "Neural Network-Based Adaptive Controller for Trajectory Tracking of Wheeled Mobile Robots," IEEE Access, vol. 10, pp. 13582–13597, 2022, https://doi.org/10.1109/ACCESS.2022.3146970..

[5] I. A. Hameed *et al.*, "A New Nonlinear Dynamic Speed Controller for a Differential Drive Mobile Robot," *Entropy*, vol. 25, no. 3, Mar. 2023, Art. no. 514, https://doi.org/10.3390/e25030514.

[6] F. Hamerlain, K. Achour, T. Floquet, and W. Perruquetti, "Higher Order Sliding Mode Control of wheeled mobile robots in the presence of sliding effects," in *Proceedings of the 44th IEEE Conference on Decision and Control*, Dec. 2005, pp. 1959-1963, https://doi.org/10.1109/CDC.2005.1582447.

[7] R. C. Dorf and R. H. Bishop, *Modern control systems*, 14th ed. Global Edition. Harlow: Pearson, 2022.

[8] A. S. Alkabaa, O. Taylan, M. Balubaid, C. Zhang, and A. Mohammadzadeh, "A practical type-3 Fuzzy control for mobile robots: predictive and Boltzmann-based learning," *Complex & Intelligent Systems*, vol. 9, no. 6, pp. 6509–6522, Dec. 2023, https://doi.org/10.1007/s40747-023-01086-4.

[9] M. Cui, H. Liu, X. Wang, and W. Liu, "Adaptive Control for Simultaneous Tracking and Stabilization of Wheeled Mobile Robot with Uncertainties," *Journal of Intelligent & Robotic Systems*, vol. 108, no. 3, July 2023, Art. no. 46, https://doi.org/10.1007/s10846-023-01908-0.

[10] G. Oriolo, A. De Luca, and M. Vendittelli, "WMR control via dynamic feedback linearization: design, implementation, and experimental validation," *IEEE Transactions on Control Systems Technology*, vol. 10, no. 6, pp. 835-852, Nov. 2002, https://doi.org/10.1109/TCST.2002.804116.

[11] A.M. D. Tran and T. V. Vu, "Robust MIMO LQR Control with Integral Action for Differential Drive Robots: A Lyapunov-Cost Function Approach," *Engineering, Technology & Applied Science Research*, vol. 15, no. 4, pp. 24775-24781, Aug. 2025, https://doi.org/10.48084/etasr.11583.

[12] J. Moreno-Valenzuela, L. Montoya-Villegas, R. Pérez-Alcocer, and J. Sandoval, "A family of saturated controllers for UWMRs," *ISA Transactions*, vol. 100, pp. 495-509, May 2020, https://doi.org/10.1016/j.isatra.2020.01.007.

[13] F.-G. Wang, H.-M. Wang, S.-K. Park, and X.-S. Wang, "Linear pole-placement anti-windup control for input saturation nonlinear system based on Takagi Sugeno fuzzy model," *International Journal of Control, Automation and Systems*, vol. 14, no. 6, pp. 1599-1606, Dec. 2016, https://doi.org/10.1007/s12555-015-0169-x.

[14] S. B. Joseph, E. G. Dada, A. Abidemi, D. O. Oyewola, and B. M. Khammas, "Metaheuristic algorithms for PID controller parameters tuning: review, approaches and open problems," *Heliyon*, vol. 8, no. 5, Art. no. e09399, May 2022, https://doi.org/10.1016/j.heliyon.2022.e09399.

[15] X.-S. Yang, *Nature-inspired optimization algorithms*, 1st ed. Amsterdam Waltham, MA: Elsevier, 2014.

[16] A.-M. D. Tran, T.-V. Vu, and Q.-D. Nguyen, "A Study on General State Model of Differential Drive Wheeled Mobile Robots," *Journal of Advanced Engineering and Computation*, vol. 7, no. 3, Sept. 2023, Art. no. 174, https://doi.org/10.55579/jaec.202373.417.

[17] H. K. Khalil, *Nonlinear Systems*, 3rd ed. Upper Saddle River, NJ: Prentice Hall, 2002.

[18] K. J. Åström and T. Hägglund, *PID controllers: theory, design, and tuning*, 2nd ed. Research Triangle Park, NC: Instrument Society of America, 1995.

[19] X. S. Yang, "Flower Pollination Algorithm for Global Optimization," in *Unconventional Computation and Natural Computation*, Springer Berlin Heidelberg, 2012, vol. 7445, pp. 240-249, https://doi.org/10.1007/978-3-642-32894-7_27.

[20] G. Kaczmarczyk, R. Stanisławski, Ł. Knypiński, D. D. Ferreira, and M. Kamiński, "Flower pollination algorithm optimization applied for Lyapunov-based fuzzy logic speed controller of a complex drive system," *Bulletin of the Polish Academy of Sciences Technical Sciences*, vol. 73, no. 5, Apr. 2025, Art. no. 154205, https://doi.org/10.24425/bpasts.2025.154205.

[21] N. H. Rohiem, A. Soeprijanto, and M. Syai'in, "Enhancing Voltage Stability under GCC Constraints with the AI-Driven Optimization of Distributed Generators," *Engineering, Technology & Applied Science Research*, vol. 15, no. 5, pp. 28063-28070, Oct. 2025, https://doi.org/10.48084/etasr.12532.